A New Probabilistic Tsunami Hazard Assessment for Australia

Gareth Davies[1]
[1] Geoscience Australia, Canberra, Australia; gareth.davies@ga.gov.au

Abstract
The 2018 Australian Probabilistic Tsunami Hazard Assessment (PTHA18) was developed by Geoscience Australia to better understand Australia's tsunami hazard due to earthquakes in the Pacific and Indian Oceans. The PTHA18 contains over a million hypothetical earthquake-tsunami scenarios, with associated return periods which are constrained using historical earthquake data and long-term plate tectonic motions. The tsunami propagation is modelled globally for 36 hours, and results are stored at thousands of sites in deep waters offshore of Australia. Average Return Interval (ARI) estimates are also provided, along with a representation of the associated uncertainties. ARI uncertainties tend to be large because of fundamental limitations in current scientific knowledge regarding the frequency of large earthquakes on global subduction zones.

The PTHA18 provides a nationally consistent basis for earthquake-tsunami scenario design, as required for inundation hazard assessments. The results and source-code are also freely available. The current paper aims to provide a short and accessible introduction to the PTHA18 methodology and results, while deliberately limiting technical details which are covered extensively in the associated technical report and code repository.

Keywords: Tsunami, Earthquake, Probabilistic Hazard Assessment

1. Introduction

More than 30 tsunamis were recorded in Australia since 1950, with the larger inducing locally significant inundation and hazardous marine currents [1, 3, 15, 22]. The majority of historical tsunamis in Australia with known sources were generated by distant earthquakes [15]. Being relatively distant from major subduction zones, Australia is not subject to "near-field" subduction earthquake-generated tsunami impacts which occur within 1000 km of the source, and have historically been the most destructive. Well-known examples of such near-field tsunami impacts include the 2004 Indian Ocean tsunami in Aceh, Indonesia, and the 2011 Tohoku tsunami in the Sendai Plain, Japan.

Although distant from major subduction zones, Australia may not be immune to damaging earthquake-generated tsunami inundation [1]. Large subduction earthquakes can produce highly directional tsunamis with the potential for "far-field" trans-oceanic impacts, depending on the earthquake's location and orientation (Figure 1). For instance the 1960 magnitude 9.5 Chile earthquake generated a tsunami with 10 m of runup in Hawaii, a distance of 11,000 km from the source. It also produced 8 m of runup in Japan at 17,000 km from the source. The death toll was respectively 61 (Hawaii) and 142 (Japan) [20]. Similarly the 2004 magnitude 9.1 Sumatra earthquake generated an Indian Ocean wide tsunami. This had 5-9 m of runup in Somalia, 5000 km from the earthquake source, where there were approximately 300 deaths [12]. The 1946 magnitude 8.6 Aleutian Islands earthquake also produced a tsunami with major far-field impacts, including 159 deaths in Hawaii (4000 km from the source) and runup reaching 20 m in the Marquesas Islands (7000 km from the source) [19]. Clearly, some tsunamis can be very hazardous even far from the earthquake source.

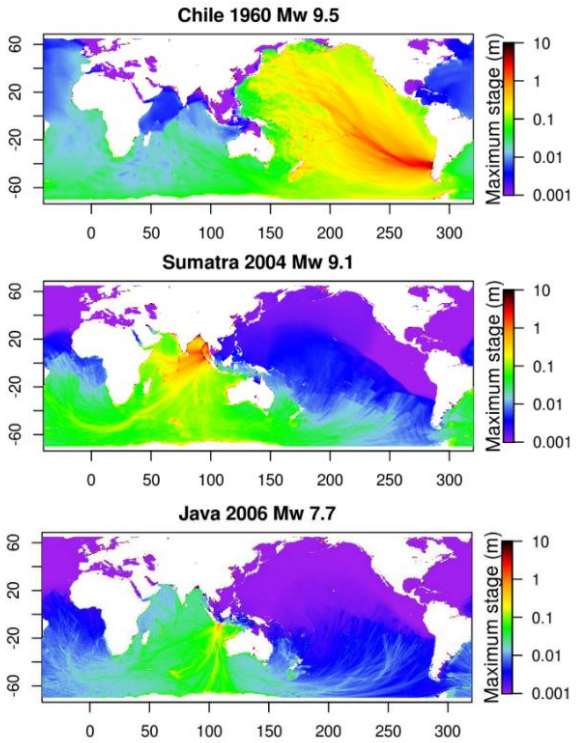

Figure 1: Modelled maximum stage (i.e. perturbation above sea-level) for three historical tsunamis: (Top) 1960 Chile Earthquake; (Middle) 2004 Sumatra-Andaman Earthquake; (Bottom) 2006 Java Earthquake. Results were derived by computing the earthquake-induced ocean-surface perturbation from slip inversions [2, 13, 21]. This was used as an initial condition (perturbation relative to ambient sea-level) for the PTHA18 tsunami propagation model [9].

The aforementioned tsunamis had relatively small impacts on Australia because most far-field energy was directed elsewhere. The Chile and Sumatra events induced marine hazards on the Australian east and west coast respectively (e.g. unusual currents, damages to boats [1]), but led to relatively minor inundation. However, earthquakes with other subduction source locations could more efficiently direct tsunami energy to Australia. For instance, the 2006 magnitude 7.7 Java earthquake produced Australia's largest historically observed tsunami runup (7.9 m at Steep Point, near Shark Bay in WA) [22] despite the earthquake magnitude being much smaller than the Chile and Sumatra events (Figure 1). This tsunami inundated some coastal campsites in central Western Australia, but the region is sparsely populated and impacts were small overall [22]. Nonetheless, this event demonstrates the importance of tsunami directivity for Australia. A larger earthquake in the same location would likely have more significant impacts on Western Australia.

The management of tsunami hazards is generally informed by site-specific inundation hazard assessments [1]. Such studies typically model the inundation associated with one or more hypothetical tsunami scenarios at a site of interest, and often average-return-intervals (ARIs) are estimated for each scenario [5, 7]. Inundation models tend to be computationally intensive and require high-resolution elevation data, so for practical reasons inundation hazard studies are generally developed on a site-by-site basis (for instance, modelling inundation over tens of kilometres of coastline, rather than at national scales) [1].

The results of tsunami inundation hazard assessments depend on two critical factors:

1) The design of the tsunami scenarios; and
2) The accuracy of the coastal hydrodynamic model.

A key challenge is the great uncertainty associated with tsunami scenario design [1]. Scenario details such as the earthquake location, magnitude and spatial distribution of slip on the fault plane can strongly affect the modelled tsunami size. Unfortunately on most global subduction zones there is large uncertainty as to the maximum possible earthquake magnitude; the ARIs of high magnitude earthquakes; and the distribution of fault-plane slip (which is only partly constrained by the earthquake magnitude). These uncertainties are widely acknowledged nowadays in the global tsunami hazard community, in part due to widespread under-estimation of maximum-magnitudes in the region of the 2011 Japan earthquake, and the surprisingly high near-trench slip observed during that event [16, 17]. Such 'surprises' reflect limitations in current-day scientific knowledge of subduction earthquake mechanics, and the fact that historical earthquake records are short (centuries or less) relative to the ARIs expected for very high magnitude earthquakes.

To illustrate just how significant these uncertainties can be, consider the Kermadec-Tonga trench, which is approximately 3000 km east of Australia and extends from New Zealand to just south of Samoa. The Global Earthquake Model Foundation recently proposed uncertainty ranges for maximum earthquake magnitudes on most subduction zones based on literature and multi-expert consensus [4]. On the Kermadec-Tonga trench the maximum magnitude ranged from 8.1 to 9.6. The lower limit approximates the largest instrumentally observed earthquakes, while the upper limit approximates to the largest historically observed earthquake magnitude anywhere (the 1960 Chile earthquake). This range reflects limitations in scientific knowledge of subduction earthquakes, and is indicative of multi-expert opinion. Even without tsunami modelling, it is clear that the maximum-magnitude range implies a "worst-case tsunami" somewhere between "a locally significant event with minor impacts on Australia" (for magnitude 8.1), up to "a Pacific-Ocean wide tsunami with substantial inundation potential in eastern Australia" (for magnitude 9.6). Other subduction zones of significance for Australia are subject to comparable uncertainties, such as the eastern Sunda Arc near Java, Indonesia.

Currently there is no standardised approach for integrating such uncertainties in tsunami hazard assessments [16]. This means subjective modelling decisions can have a substantial influence on inundation hazard assessments, and it is non-trivial to compare scenarios and return periods devised by different practitioners. This is a problem for risk management purposes, where it is desirable to have a consistent view of the hazard at state and national scales, as well as a consistent view of the associated uncertainties.

To facilitate national consistency in the assessment of Australia's tsunami hazard, Geoscience Australia recently published the 2018 Australian Probabilistic Tsunami Hazard Assessment (henceforth PTHA18) [9]. The PTHA18 is a nationally consistent "offshore" tsunami hazard assessment for Australia. It currently only considers distant earthquake sources, although other potential tsunami sources do exist (e.g. submarine landslides) [1]. The purpose of the PTHA18 is to provide a nationally consistent source of earthquake-tsunami scenarios and ARIs, with quantification of the associated uncertainties. The tsunamis are simulated offshore, but the results can be combined with site-specific inundation models at any location around Australia to conduct tsunami inundation hazard assessments. This article provides a brief overview of the PTHA18, suppressing technical details for brevity

(see [9] for a more comprehensive exposition of the study and links to the associated source-code).

2. The 2018 Australian Probabilistic Tsunami Hazard Assessment (PTHA18)

2.1 Earthquake-tsunami scenarios

The PTHA18 includes earthquake-tsunami scenarios from major earthquake source-zones in the Pacific and Indian Oceans (Figure 2). Each source-zone has an associated non-uniform fault-plane geometry, on which earthquake slip occurs. On most source-zones only thrust earthquakes are modelled, although a number of smaller normal-fault earthquake sources close to Australia are included.

Each source-zone is represented as a curvilinear grid of "unit-sources", which partition the fault geometry into pieces of approximately 50 x 50 km^2 (Figure 2). All earthquake scenarios are represented as linear combinations of slip on the unit-sources (bottom panels of Figure 2). The scenario earthquake magnitudes range in increments of 0.1, between 7.2 and a source-zone specific upper-limit that reflects the uncertainty of the maximum magnitude. This upper magnitude limit increases with the source-zone area (because large magnitude earthquakes are expected to require large areas), but is always less than or equal to 9.6 (as in [4, 8]). For any given magnitude the database contains hundreds to thousands of earthquake scenarios on each source-zone. Larger source-zones generally have more scenarios because their fault area offers a greater number of potential earthquake locations.

Because there is uncertainty as to how earthquake scenarios should be modelled, the PTHA18 includes tests of several different approaches. No single approach was *a-priori* assumed to give a good representation of real tsunamis; rather, their empirical performance was tested as part of the study (below). The simplest approach is termed fixed-area-uniform-slip or FAUS, and represents earthquake scenarios with uniform slip over a prescribed rupture area which is deterministically related to the earthquake magnitude (bottom-left panel of Figure 2). FAUS-like approaches are common in tsunami hazard studies (although they are not recommended for use in PTHA18, see discussion below). Earthquake observations suggest a roughly exponential relationship between magnitude and rupture area, but with substantial additional variability which is not represented by the FAUS approach. To represent this we also tested a set of variable-area-uniform-slip (VAUS) scenarios, which have uniform-slip combined with an approximate factor-of-ten stochastic variation in rupture area for a given magnitude. If the magnitude is fixed, then VAUS scenarios with smaller area have higher slip, which increases the variability of tsunamis generated by VAUS scenarios, as compared with FAUS scenarios. Finally we also tested a set of heterogeneous-slip (HS) scenarios (bottom right of Figure 1). Spatial variations in slip are well known to have an important impact on tsunamis in the near-field, and a number of studies suggested they also affect tsunamis far from the source, which motivated the inclusion of HS scenarios in our database. The random slip model was previously tested by comparison with 66 earthquake finite-fault inversions [10]. The PTHA18 database contains around 750,000 HS scenarios, a similar number of VAUS scenarios, and around 50,000 FAUS scenarios.

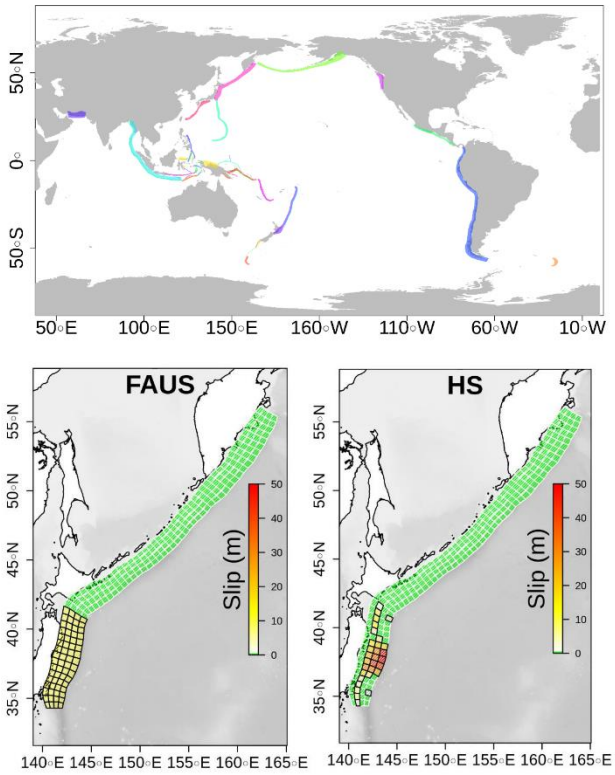

Figure 2: (Top) Earthquake source locations included in the PTHA18 [9]. (Bottom) Two hypothetical earthquake scenarios close to Japan. All scenarios are represented as linear combinations of unit-sources. The left-hand-side depicts a fixed-area-uniform-slip (FAUS) scenario, while the right-hand-side depicts a heterogeneous-slip (HS) scenario. See [9] for details on scenario generation.

For each earthquake scenario we computed the vertical co-seismic deformation (i.e. uplift or subsidence) generated by the earthquake slip, approximating the earth as a homogeneous elastic half-space [18]. This represents the seabed deformation. The ocean-surface deformation is derived from the seabed deformation by applying a filter based on 3D potential flow theory [14]. This represents the non-hydrostatic response of the ocean to seabed uplift by filtering out spatial wavelengths on the order of the ocean depth, while

leaving larger spatial scales unaffected. The ocean-surface deformation is then used to initialise a tsunami propagation model, as a perturbation to mean sea level. The tsunami propagation model solves the linear shallow water equations in spherical coordinates, including the Coriolis force. The model is evolved for 36 hours on a global elevation grid (similar to Figure 1). Our propagation model has a uniform 1-arc-minute spatial resolution, corresponding to grid cell sizes around 1.8 x 1.8 km^2 near the equator. The elevation data is based on a mixture of the GEBCO14 and GA250m datasets.

The computational effort is greatly reduced using a unit-source approach. This exploits the fact that our tsunami model is linear in the ocean-surface deformation, while the ocean-surface deformation model is linear in the earthquake slip. Therefore, the tsunami due to any earthquake can be computed as a linear combination of the tsunamis associated with 1 m of slip on each individual unit-source (hence the name "unit-source"). The tsunami propagation is by far the most expensive part of the above computation; using a unit-source approach we only need 1 propagation simulation per unit-source (around 4000 in total), instead of one per earthquake, which reduces the computational effort by well over 100 times.

The tsunami model results are stored at approximately 20,000 points globally (termed "hazard points"). Most hazard points are concentrated around Australia to facilitate their use for site-specific inundation hazard studies. Some global hazard points are also stored to support model testing, including at the locations of deep ocean gauges (DART buoys). The DART buoys are specifically designed for tsunami observation, and were used to test the earthquake scenario generation methodologies.

The scenarios were tested by comparison with 18 earthquake-tsunamis with magnitude >7.7, observed in 2006-2016 which were measured at DART buoys. Each tsunami was observed at between 1 and 28 DART buoys (examples in Figure 3). For each earthquake slip model (FAUS, VAUS, HS), we extracted scenarios from the PTHA18 database which have "similar earthquake magnitude and location" as each observed earthquake (see [9] for details). Ideally, each set of model scenarios would give an unbiased representation of real tsunamis with the same magnitude and location. Otherwise, the model is biased. This can be tested (for each earthquake slip model separately) by comparing the set of 18 observed events with the random model scenarios.

To this end, we firstly used a goodness-of-fit criteria to measure the agreement of each modelled scenario with the observed tsunami time-series [9]. This allowed the automated identification of PTHA18 scenarios which "most resemble" the observations (see Figure 3 for an example). Finally, the alternative earthquake slip models (VAUS, FAUS, HS) were tested for "tsunami bias" by addressing the following questions:

1) Does the set of scenarios with "similar earthquake location and magnitude as the observation" consistently include some tsunamis with reasonable agreement to observations (as in Figure 3)?
2) Are the statistical properties of the "good-fitting" model scenarios consistent with a random sample from the set of all scenarios with "similar location and magnitude" as the observation?

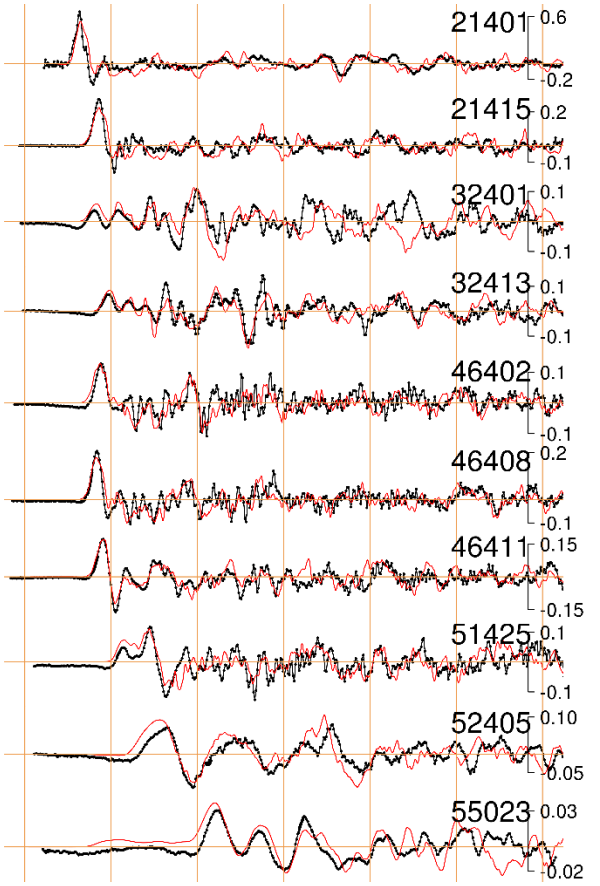

Figure 3: Deep ocean tsunami wave time series observed in the Pacific following the 2011 magnitude 9.1 Tohoku earthquake (black) are compared with a single heterogeneous-slip PTHA18 [9] scenario (red) which has similar earthquake location and magnitude, with "best-fit" according to our goodness-of-fit criteria. Units in m. The vertical lines denote one hour spacing, and the times are offset horizontally on a per-gauge basis to capture the first 5-6 hours of the wave. Numeric labels correspond to the DART-buoy gauge ID. See [9] for gauge locations, and model-vs-data comparisons for other tsunamis. See [1, 9] for further discussion of this PTHA18 scenario.

Detailed answers to these questions are presented in [9]. In brief, it was found that that both the HS and

VAUS scenarios tended to include "best-fit" tsunamis with comparable agreement to observations. The FAUS model performed more poorly, and thus FAUS scenarios are not recommended for use in tsunami hazard assessments. Furthermore, downward-biases in tsunami wave heights were identified for both uniform-slip models (FAUS and VAUS). For these uniform-slip models, the "good-fitting" scenario tsunamis tended to be large as compared to random scenario tsunamis. This indicates statistical under-estimation of tsunami size (i.e. downward bias) by the uniform-slip models. No such biases were identified for the HS model.

Based on these results, the HS scenarios are recommended for use in tsunami hazard assessments. Alternatively, we developed a technique to "bias-adjust" the VAUS model results by preferentially selecting scenarios with low rupture area and high slip, because such scenarios are disproportionately represented among VAUS scenarios which best fit observations. This was found to produce offshore hazard results similar to the HS scenarios (discussed further below). The option of using two different scenario types in hazard studies (i.e. HS, and bias-adjusted VAUS) may be useful in some situations. For example, it allows hazard assessments to represent uncertainties in "how earthquakes should be schematized". See [9] for full details.

2.2 Estimation of ARIs

Hazard assessments often use ARIs to assist with scenario selection. For instance, an inundation study may select tsunami scenarios which produce a specific ARI maximum-stage offshore of the site of interest, with the ARI set at some level (e.g. 500 or 2500 years) depending on the criticality of the application. ARIs can also be specified based on the earthquake magnitude, and the frequency with which this is exceeded on any source-zone.

Irrespective of whether the earthquake magnitude or site-specific tsunami size is used to define the ARI, the corresponding tsunami inundation is not expected to have exactly the same ARI. This is analogous the situation in flood hazard studies, where a 100 year rainfall event with 1 day duration might not produce a 100 year inundation event everywhere in the catchment, depending on the temporal and spatial details of the rainfall and the nature of the catchment itself. For tsunamis, the linkage between the offshore wave properties and inundation will vary depending on details of the waveform and the coastal morphology.

There is usually high uncertainty in the ARIs associated with large earthquakes and tsunamis, irrespective of the statistic used to define the ARI. This stems from uncertainties in key subduction-zone parameters (e.g. maximum earthquake magnitudes), and the fact that historical records are short compared with the expected frequency of the most hazardous events. A key feature of the PTHA18 methodology is that these uncertainties are quantified, while maintaining reasonable consistency with the historical earthquake record and tectonic plate convergence rates.

For the PTHA18 occurrence-rates (events/year) are assigned to each individual earthquake scenario on per-source-zone basis. To do this the source-zone's magnitude vs exceedance-rate curve is modelled, assuming it follows a Gutenberg-Richter type distribution with unknown parameters. The exceedance-rate is defined as the inverse of the ARI. The unknown source-zone parameters are the maximum earthquake magnitude, the seismic coupling (i.e. fraction of tectonic plate convergence attributable to earthquakes), and the b-value (i.e. slope of the magnitude-frequency curve). The rate of tectonic plate convergence (Figure 4) places some constraint on frequency of thrust earthquakes via the "moment conservation" principle, which states that earthquake slip balances at most 100% of plate convergence over long time periods.

The unknown Gutenberg-Richter parameters are initially assigned weakly informative prior distributions, which are consistent with the source-zone's plate convergence rates and the maximum earthquake magnitude thought to have occurred based on paleo or historical observations. For conservatism, the seismic coupling is not permitted to be less than 10%. A Bayesian technique is then used to derive 'posterior' parameter distributions based on historical earthquake data [8]. This leads to magnitude vs exceedance-rate models that are reasonably consistent with both historical observations and moment conservation, and provide some quantification of exceedance-rate uncertainties (bottom panel of Figure 4).

The rate models have been tested at the global level, and via various regional comparisons with other estimated magnitude exceedance rates, based on long term historical or paleo data. See [9] for full details. These tests suggest the methodology lead to a reasonable representation of mean exceedance rates and uncertainties, as compared with other approaches.

On large source-zones it is plausible that key parameters (such as the maximum magnitude) may vary spatially. To allow the model to represent this, we consider the possibility that some large source-zones are split into segments. In this case the "union of segments" interpretation is assigned a 50% weight, with the other 50% placed on the unsegmented model.

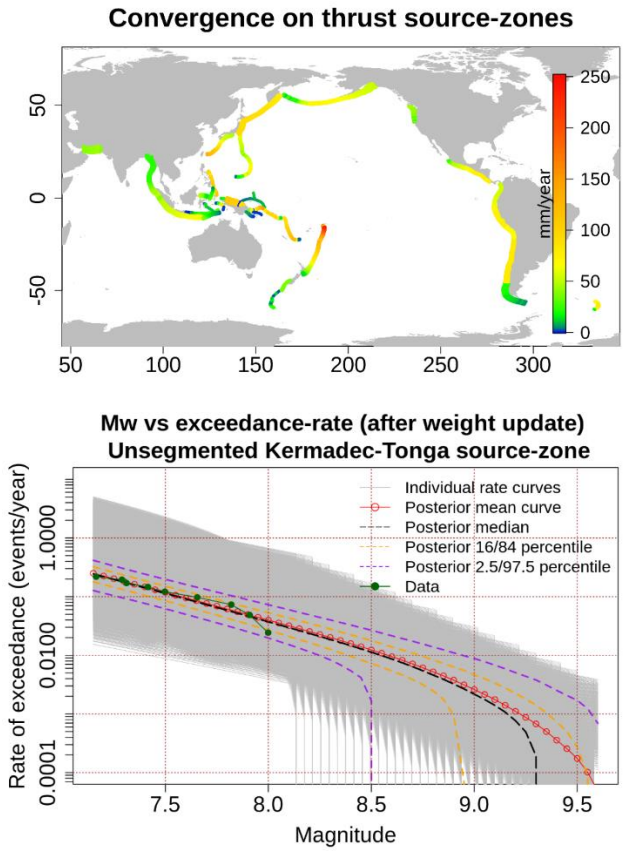

Figure 4: (Top) Spatially variable tectonic plate convergence rates (mm/year) on thrust source-zones, as input to the PTHA18 [9]. (Bottom) Example earthquake magnitude-frequency distribution and uncertainties on a source-zone, using the unsegmented Kermadec-Tonga source-zone as an example. On all source-zones the modelled magnitude exceedance-rates are constrained using both historical earthquake observations, and tectonic convergence rates. See [9] for methodological details.

The source-zone magnitude vs exceedance-rate model may be "partitioned" into individual scenario occurrence-rates. The individual scenario occurrence-rates are defined so that integration over all scenarios reproduces the full source-zone's magnitude vs exceedance-rate curve. In addition, the individual scenario occurrence-rates are made to depend on each scenario's earthquake location, such that the modelled time-integrated rate of earthquake slip approximately reproduces the spatial pattern of tectonic plate convergence (Figure 4). This provides a convenient approach to representing spatial variations in seismicity that are expected in large source-zones.

Once scenario occurrence-rates are assigned, they may be directly translated into ARI curves for any other modelled tsunami statistic of interest. For simplicity, herein we focus on the maximum-stage (i.e. maximum positive perturbation above sea level) at a large set of hazard points around Australia. The maximum-stage gives a rough indicator of the 'size' of the tsunami at a particular point. We emphasise that inundation will also depend on other aspects of the tsunami waveform and the coastal morphology. Thus we do not expect to see a precise relationship between the maximum-stage ARI offshore and the inundation-depth ARI at any nearby onshore site. However, if all else is equal we expect a greater maximum-stage to produce greater inundation, so it provides a useful tsunami-size related summary statistic.

The top panel of Figure 5 shows the 500 year maximum-stage at a set of hazard points around Australia. This uses the HS model scenarios, although similar results are obtained using the "bias-adjusted" VAUS scenarios discussed in Section 2.1.

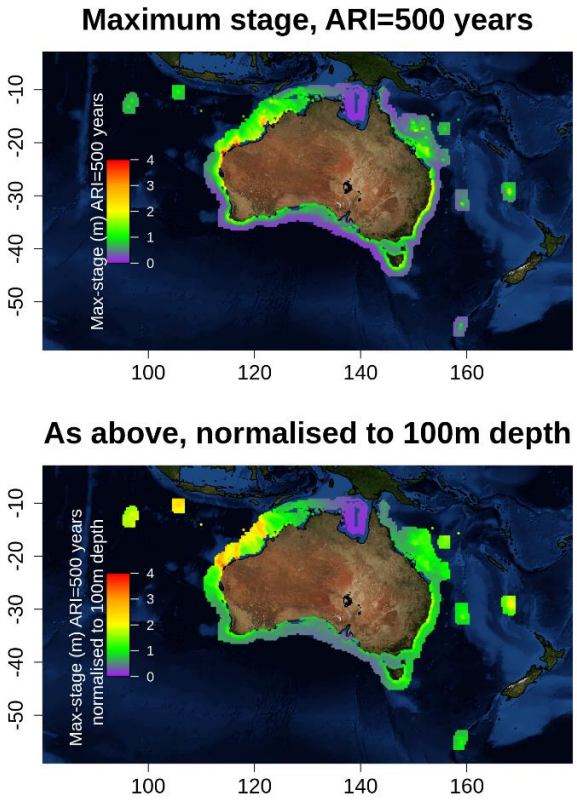

Figure 5: (Top) Maximum stage above ambient sea-level at ARI=500 years in PTHA18 [9]. (Bottom) Same result as in the top panel normalised to 100m depth using Green's law, which reduces the visual impact of wave shoaling on the results. See [9] for further details.

Due to wave shoaling, there is a clear tendency for sites closer to the coast to have larger waves than sites further offshore in deeper water. Because the tsunami was modelled using the linear shallow water equations on a 1 arc-minute grid, the results should become less accurate close to the coast where the coastal bathymetry is more poorly represented, and nonlinearity may significantly affect the hydrodynamics. To reduce the visual effects of depth variation on the results, the bottom panel of Figure 5 depicts the same result

normalised to 100 m depth using Green's law (i.e. multiplied by $(\text{depth}/100)^{0.25}$). This corrects for wave shoaling, assuming plane waves over planar topography [23]. While undoubtedly an approximation, the normalisation greatly reduces the shore-normal variation of maximum-stage and makes it practically easier to infer regional patterns in the results.

Figure 5 suggests the north-west coast of Australia has the greatest exposure to high offshore waves at ARI=500 years. This is because of its proximity to the eastern Sunda Arc about 1-2 thousand kilometres to the north (just south of Indonesia). Tsunami inundation of several metres has been historically reported in this region following three earthquakes on the eastern Sunda Arc in 1977 (magnitude 8.3), 1994 (magnitude 7.8), and 2006 (magnitude 7.7) [6]. It seems reasonable that larger magnitude earthquakes could occur on the eastern Sunda Arc, even though they were not observed historically. This is because the subduction zone is wide and rapidly converging, and because large earthquakes have historically occurred on the western Sunda Arc (e.g. resulting in the 2004 Indian Ocean tsunami).

Somewhat lower ARI=500 maximum-stage values are derived for the east coast, and the south-west coast (Figure 5). These are exposed to source-zones in the Pacific and Indian Oceans respectively, but at greater distances as compared with the north-west coast. Relatively low ARI=500 maximum-stage values are predicted for the south coast, and the north coast around the Gulf of Carpentaria (Figure 5). They are even more distant from major earthquake source-zones, with the Gulf of Carpentaria region being additionally sheltered by landmasses.

Large uncertainties in the frequency of high magnitude earthquakes (as represented in the lower panel of Figure 4) should obviously translate into large uncertainties in the maximum-stage at a given ARI. To quantify this we use the Bayesian uncertainties in the magnitude vs exceedance-rate curves. For instance, Figure 4 depicts the 2.5%, 16%, 50%, 84% and 97.5% posterior percentile curves for the unsegmented Kermadec-Tonga source. We may hypothesise that any one of these represents the "real" magnitude vs exceedance-rate curve, and use the aforementioned method to partition the exceedance-rates among individual scenarios. By doing this on all source-zones, one may derive percentile uncertainties for the maximum-stage values at a given ARI.

A complication arises in such uncertainty calculations, because systematic errors may be correlated between source-zones. For instance, if a "low percentile" of our magnitude vs exceedance-rate model turns out to be correct on the Kermadec-Tonga source-zone, does this affect the likelihood that a "low percentile" is also correct on the New-Hebrides source-zone, or anywhere else? A-priori some kind of dependence seems likely. For example, it would not be surprising if our mean model turned out to consistently over-estimate (or under-estimate) the exceedance-rates of high magnitude earthquakes on source-zones which share similar physical properties, due to some underlying physical mechanism that is not treated in the model (but may be established by future science). While obviously difficult to specify, independence of the uncertainties seems unlikely. Therefore, in the PTHA18 we employ a co-monotonic model of inter-source-zone uncertainty dependence. This approach has previously been applied to tsunami hazard, and is more generally used to robustly model dependence to support decisions under risk and uncertainty [8, 11].

Figure 6 gives an example of the resulting 16th and 84th percentile uncertainties for the maximum-stage at ARI=500 years, normalised to 100 m depth for visual clarity. The plot gives an indication of how our estimated ARI=500 maximum-stage might change in future, as our understanding of subduction earthquake frequencies is refined with better data.

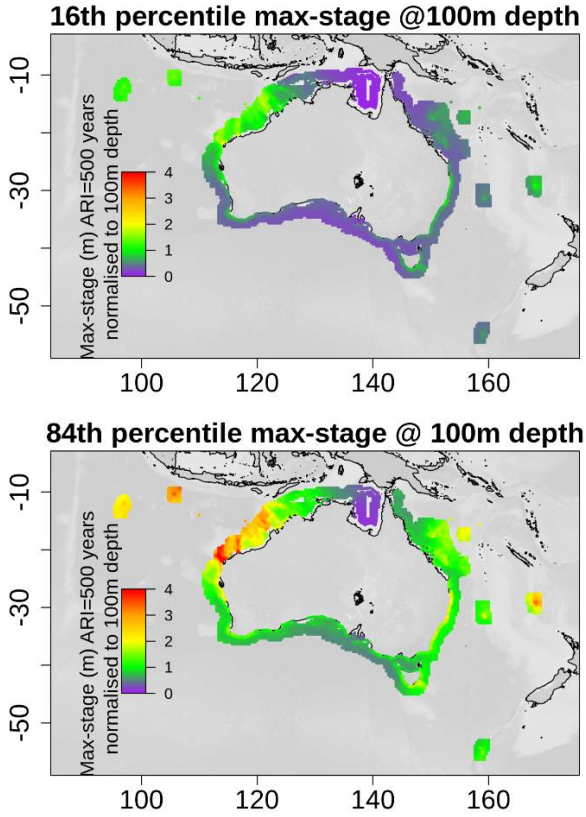

Figure 6: Uncertainties in the PTHA18 [9] ARI=500 year maximum-stage normalised to 100m depth, represented using the 16th percentile (top) and the 84th percentile (bottom). See Figure 5 for the mean, and [9] for further details.

The uncertainties in Figure 6 are large, with the maximum stage often varying around a factor of two between the 16th and 84th percentiles. This should not be surprising given the fundamentally uncertain frequencies of large earthquakes on most source-zones. For example on the unsegmented Kermadec-Tonga source (Figure 4), earthquakes with magnitude > 9 are impossible at the 16th percentile uncertainty, but occur on average every few hundred years at the 84th percentile. Clearly large uncertainties in the maximum-stage at a given ARI should be expected in this situation.

2.3 Hazard-deaggregation

In tsunami inundation applications it may be computationally challenging to simulate a large number of scenarios from the PTHA18. It is the responsibility of inundation modellers to decide on scenario selection techniques for their study. The way this is done may vary from study to study depending on the purpose of the modelling, and the extent to which modelled nearshore flows at the site of interest are sensitive to variations in the offshore tsunami wave form. We suggest that inundation modellers consult [1] for further information on the design of inundation studies.

Although there is no "general solution" to the scenario selection problem, a number of products are provided in the PTHA18 to assist with the process. In addition to ARI information and uncertainties at all offshore points, we provide "hazard-deaggregation plots" such as in Figure 7. For a given hazard point, this gives a visual depiction of the likely locations of earthquakes that would generate a tsunami at the hazard point with maximum-stage greater than some specified threshold (one may alternatively specify an ARI, rather than a maximum-stage). For instance Figure 7 suggests that a tsunami exceeding the 1/100 maximum-stage offshore of Sydney could be generated from a range of sources, most prominently in parts of the Kermadec-Tonga, South-America, Puysegur and southern New Hebrides subduction zones. To create these plots we firstly select all PTHA18 scenarios that have maximum-stage above the chosen threshold at the hazard point. Each of these has a mean occurrence-rate, and that rate is partitioned between its unit-sources in proportion to their slip. We then sum over all scenarios on each unit-source, leading to a single number for each unit-source which is used to colour Figure 7.

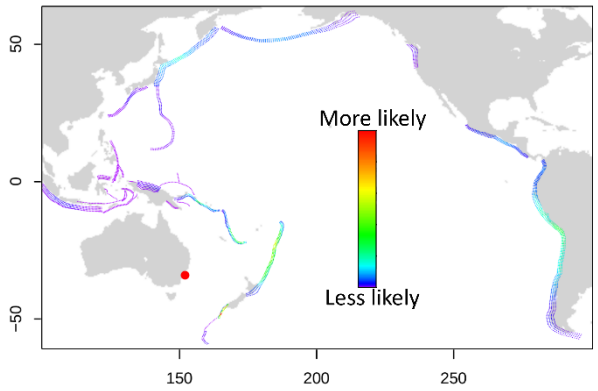

Figure 7: Example hazard-deaggregation plot for a point offshore of Sydney (red dot) in PTHA18 [9]. The source-zones are coloured based on the relative likelihood that they would host an earthquake which generates a 1/100 year tsunami maximum-stage at the Sydney point.

3. Summary

The PTHA18 provides a nationally consistent source of distance-earthquake tsunami scenarios for all of Australia, along with ARI information. The tsunami scenarios have been tested by comparison with 18 observed events, giving consideration to both "whether events that look like observations occur in the database", and "whether the statistical properties of the scenarios are consistent with observations". The ARI information has been derived based on historical earthquake catalogues and tectonic convergence rates, with tests suggesting it gives a reasonable depiction of earthquakes frequencies. However, there is unavoidably very large uncertainty as to the frequency of high-magnitude earthquakes, because of limitations in current-day scientific understanding of subduction zones. This places fundamental constraints on our ability to precisely quantify tsunami hazards. Nonetheless the PTHA18 offers a nationally consistent representation of these uncertainties, which can assist with making tsunami inundation hazard results more comparable at different sites around Australia.

The PTHA18 report [9], results, and source-code are freely available. For information on how to access this, see www.ga.gov.au/ptha.

4. Acknowledgements

This paper is published with the permission of the CEO, Geoscience Australia. The PTHA18 was undertaken with the assistance of resources from the National Computational Infrastructure (NCI), which is supported by the Australian Government.

5. References

[1] AIDR (2018). Tsunami hazard modelling guidelines. Australian Institute of Disaster Resilience, https://knowledge.aidr.org.au/media/5640/tsunami-planning-guidelines.pdf

[2] Ammon, C. J., Kanamori, H., Lay, T. and Velasco, A. A. (2006) The 17 July 2006 Java tsunami earthquake. Geophysical Research Letters, 33, 1-5.

[3] Beccari, B. (2009) Measurements and Impacts of the Chilean Tsunami of May 1960 in New South Wales, Australia. NSW State Emergency Service.

[4] Berryman, K., Wallace, L., Hayes, G., Bird, P., Wang, K., Basili, R., Lay, T., Pagani, M., Stein, R., Sagiya, T., Rubin, C., Barreintos, S., Kreemer, C., Litchfield, N., Stirling, M., Gledhill, K., Haller, K. and Costa, C. (2015) The GEM Faulted Earth Subduction Interface Characterisation Project: Version 2.0 – April 2015. Global Earthquake Model.

[5] Boswood, P. K. (2013) Tsunami Modelling along the East Queensland Coast. Proceedings of Australasian Coasts and Ports 2013, Manly, NSW, Australia.

[6] Burbidge, D. and Cummins, P. (2007) Assessing the threat to Western Australia from tsunami generated by earthquakes along the Sunda Arc. Natural Hazards, 43, 319-331

[7] Cardno, (2013). NSW Tsunami Inundation Modelling and Risk Assessment. NSW State Emergency Service and the Office of Environment and Heritage.

[8] Davies, G., Griffin, J., Løvholt, F., Glimsdal, S., Harbitz, C., Thio, H. K., Lorito, S., Basili, R., Selva, J., Geist, E. and Baptista, M. A. (2017) A global probabilistic tsunami hazard assessment from earthquake sources Geological Society of London Special Publications SP456.5

[9] Davies, G. and Griffin, J. (2018). The 2018 Australian Probabilistic Tsunami Hazard Assessment: Hazards from earthquake generated tsunamis. Geoscience Australia Record 2018/41. http://dx.doi.org/10.11636/Record.2018.041

[10] Davies, G., Horspool, N., and Miller, V. (2015) Tsunami inundation from heterogeneous earthquake slip distributions: Evaluation of synthetic source models. Journal of Geophysical Research: Solid Earth. 120, 6431-6451.

[11] Deelstra, G. and Dhane, J. and Vanmaele, M. (2009) An overview of comonotonicity and its applications in finance and insurance. Advanced Mathematical Methods for Finance, Springer.

[12] Fritz, H. M. and Borrero, J. C. (2006) Somalia Field Survey after the December 2004 Indian Ocean Tsunami. Earthquake Spectra, 22, 219-233.

[13] Fuji, Y. and Satake, K. (2013) Slip distribution and seismic moment of the 2010 and 1960 Chilean Earthquakes Inferred from Tsunami Waveforms and Coastal Geodetic Data. Pure and Applied Geophysics, 170, 1493-1509.

[14] Glimsdal, S., Pedersen, G., Harbitz, C. and Løvholt, F. (2013) Dispersion of tsunamis: does it really matter? Natural Hazards and Earth System Sciences, 13, 1507-1526

[15] Goff, J. and Chague-Goff, C. (2014). The Australian tsunami database: A review. Progress in Physical Geography, 2014, 38, 218-240.

[16] Grezio, A., Babeyko, A., Baptista, M. A., Behrens, J., Costa, A., Davies, G., Geist, E. L., Glimsdal, S., Gonzalez, F. I., Griffin, J., Harbitz, C. B., LeVeque, R. J., Lorito, S., Lovholt, F., Omira, R., Mueller, C., Paris, R., Parsons, T., Polet, J., Power, W., Selva, J., Sorenson, M. B and Thio, H. K. (2017) Probabilistic Tsunami Hazard Analysis: Multiple Sources and Global Applications. Reviews of Geophysics, 55, 1158-1198.

[17] Kagan, Y. Y. and Jackson, D. D. (2013) Tohoku Earthquake: A Surprise? Bulletin of the Seismological Society of America, 103, 1181-1194

[18] Okada, Y. (1985) Surface deformation due to shear and tensile faults in a half-space. Bulletin of the Seismological Society of America, 75 , 1135-1154

[19] Okal, E. A., Synolakis, C. E., Fryer, G. J., Heinrich, P., Borrero, J. C., Ruscher, C., Arcas, D., Guille, G., and Rousseau, D. (2002) A Field Survey of the 1946 Aleutian Tsunami in the Far Field. Seismological Research Letters, 73, 490-503

[20] Okal, E. A. (2011) Tsunamigenic Earthquakes: Past and Present Milestones. Pure and Applied Geophysics 168, 969-995

[21] Piatanesi, A. and Lorito, S. (2007). Rupture Process of the 2004 Sumatra-Andaman Earthquake from Tsunami Waveform Inversion. Bulletin of the Seismological Society of America, 97, S223-S231

[22] Prendergast, A. and Brown, N. (2012) Far-field impact and coastal sedimentation associated with the 2006 Java tsunami in West Australia. Natural Hazards, 60, 69-79.

[23] Synolakis, C. E. (1991) Green's law and the evolution of solitary waves. Physics of Fluids, 3, 490-491.